BULLETIN OF THE POLISH ACADEMY OF SCIENCES
TECHNICAL SCIENCES, Vol. 61, No. 3, 2013
DOI: 10.2478/bpasts-2013-0079

GaInNAs quantum-well vertical-cavity surface-emitting lasers emitting at 2.33 μm

Ł. PISKORSKI and R.P. SARZAŁA*

Photonics Group, Institute of Physics, Lodz University of Technology, 219 Wolczanska St., 90-924 Lodz, Poland

Abstract. In the present paper, the comprehensive fully self-consistent optical-electrical-thermal-recombination model is used to determine the optimal structure of the possible GaInNAs quantum-well (QW) tunnel-junction (TJ) vertical-cavity surface-emitting lasers (VCSELs) with single-fundamental-mode operation at 2.33 μm wavelength suited for carbon monoxide sensing applications. From among various considered structures, the diode laser with 4-μm TJ and two 6-nm $Ga_{0.15}In_{0.85}N_{0.015}As_{0.985}/Ga_{0.327}In_{0.673}As_{0.71}P_{0.29}$ QWs has the lowest threshold current and seems to be optimal for the above applications. Higher threshold currents are obtained for $Ga_{0.15}In_{0.85}N_{0.015}As_{0.985}/Al_{0.138}$-$Ga_{0.332}In_{0.530}As$ QW structures but the latter can be grown in reactors without P source which are used for fabrication of GaAs-based devices. Both the modelled VCSELs offer a very promising room temperature continuous wave performance and may represent an alternative choice to GaSb-based lasers.

Key words: simulation of a diode laser operation, QW VCSELs, mid-infrared radiation, dilute nitrides.

1. Introduction

There is now increasing interest in room temperature (RT) continuous wave (CW) regime of the mid-infrared semiconductor devices due to their possible applications such as distant air monitoring, medical diagnostics, wireless optical communication, thermovision measurements, and laser spectroscopy [1, 2]. Semiconductor lasers emitting radiation of wavelengths longer than 2 μm are currently produced with the aid of the GaSb technology [3], however manufacturing of GaSb structures is relatively expensive and complex, thermal conductivities of GaSb-based semiconductors [4–7] are disappointedly low, carrier confinement in GaSb active regions [8, 9] is relatively low and GaSb substrates [10] are still expensive and of limiting sizes. The alternate substrate material is InP which is much cheaper than GaSb. Furthermore, InP-based devices can be manufactured using well known, much simpler and less expensive technology. Therefore, there is a wide interest to replace in the above applications the GaSb lasers with the InP-based ones produced using diluted nitrides as, for example, InNAs, GaInNAs, and GaInNAsSb.

Dilute nitride alloys have some unusual properties in comparison with most known semiconductors. An increase in their nitride contents leads to reductions of both the lattice constant and the energy gap. Therefore, choosing properly the mole fractions of indium and nitrogen, the strain within these nitride structures and their band gaps can be controlled as far as the layer thickness remains below a critical limit for creation of misfit dislocations. In the GaAs-based VCSELs, their application enables reaching both the 1.31-μm and the 1.55-μm emission bands [11] used in the fiber-optic communication. Advanced InP-based technology, on the other hand, is expected to reach even the 3.5-μm emission.

In the present paper, the comprehensive fully self-consistent optical-electrical-thermal-recombination model is used to determine optimal structure of the possible GaInNAs quantum-well (QW) tunnel-junction (TJ) vertical-cavity surface-emitting lasers (VCSELs). The target wavelength equal to 2.33 μm is selected in order to cover a strong absorption line of carbon monoxide (CO) [12] (Fig. 1).

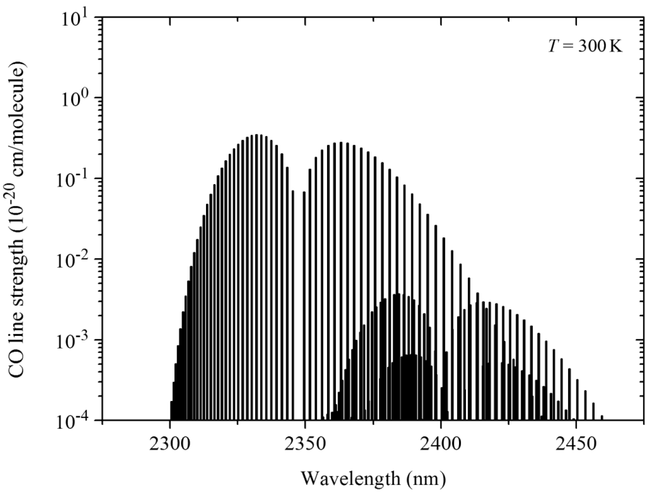

Fig. 1. Absorption lines of CO as a function of wavelength

2. The structure

A general concept of the modelled structure (Fig. 2) is similar to the currently most modern 2.33-μm GaInAsSb/AlGaAsSb GaSb-based VCSEL proposed in [13–15]. Its intentionally undoped active region is assumed to be composed of 6-nm $Ga_{0.15}In_{0.85}N_{0.015}As_{0.985}$ QWs separated by 10-nm $Ga_{0.327}In_{0.673}As_{0.71}P_{0.29}$ (laser A) or $Al_{0.138}Ga_{0.332}$-

*e-mail: robert.sarzala@p.lodz.pl

$In_{0.530}As$ (laser B) internal barriers. External 30-nm barriers manufactured from the same material as the internal ones are assumed on both active-region sides. The active region is sandwiched by InP (laser A) or $Ga_{0.47}In_{0.53}As$ (laser B) spacers, doped with silicon ($5\cdot10^{17}$ cm^{-3}) or zinc ($5\cdot10^{17}$ cm^{-3}) on the n and p sides, respectively. Above p-type spacer, the TJ composed of 15-nm p^{++}-$Al_{0.21}Ga_{0.26}In_{0.53}As$ doped with carbon ($2\cdot10^{19}$ cm^{-3}) and 15-nm n^{++}-$Al_{0.21}Ga_{0.26}In_{0.53}As$ doped with silicon ($2\cdot10^{19}$ cm^{-3}) is located. To minimise the absorption loss, the TJ is situated at the standing-wave node. Upper spacer is manufactured from InP (laser A) or $Ga_{0.47}In_{0.53}As$ (laser B) doped with silicon up to $5\cdot10^{17}$ cm^{-3}. The 3-λ cavity is terminated on both sides by distributed-Bragg-reflectors (DBRs): the 4-pair α-Si (162 nm)/SiO_2 (407 nm) top DBR and the fused 36.5-pair GaAs (175 nm)/$Al_{0.90}Ga_{0.10}As$ (200 nm) bottom DBR. The bottom DBR is doped with silicon up to $2\cdot10^{18}$ cm^{-3} ($Al_{0.90}Ga_{0.10}As$) and $5\cdot10^{17}$ cm^{-3} (GaAs). Bottom DBR diameter is assumed to be equal to 60 μm, whereas the upper DBR diameter is larger by 6 μm than TJ diameter. The top contact is produced in a form of a ring of 10 μm width. It is separated from the top spacer with the 200-nm thick highly silicon-doped ($5\cdot10^{18}$ cm^{-3}) n^+- $Ga_{0.47}In_{0.53}As$ contact layer. The whole bottom 60 μm diameter surface of the 200-μm GaAs substrate doped with silicon up to $2\cdot10^{18}$ cm^{-3} is covered by the bottom contact. The laser is attached to the cylindrical (height = diameter = 5 mm) copper heat sink with 3-μm indium solder.

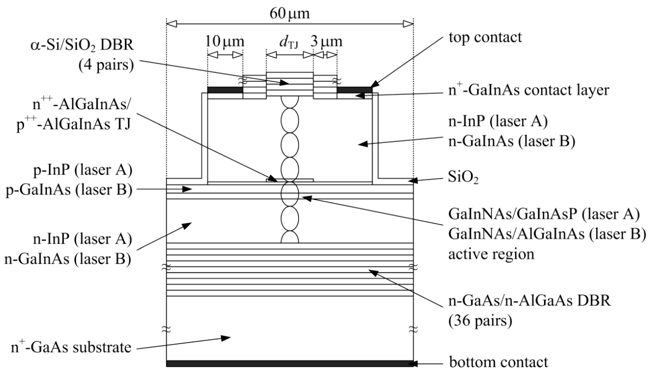

Fig. 2. The 2.33-μm QW TJ-VCSEL structure under consideration

3. The model

To simulate RT CW threshold operation of the GaInNAs QW TJ-VCSEL, we have adapted, our three-dimensional optical-electrical-thermal-recombination self-consistent model reported earlier by Sarzała and Nakwaski [16]. The model consists of four mutually interrelated parts:

a) The finite-element (FE) electrical model [17,18] characterizes both the current spreading including carrier drift and diffusion processes within the device volume between the top and the bottom contacts, the injection of both electrons and holes into the active region, and their radial diffusion within it before their monomolecular, bimolecular and Auger recombinations.
b) The FE thermal model [17,19] gives details of a heat generation nonradiative recombination, reabsorption of radiation as well as the volume and the barrier Joule heating and its spreading from the heat sources toward the heat sink and within it.
c) The optical model describes, for successive radiation modes, optical fields within the resonator. The model is based on the effective frequency method [20]. The lasing threshold is determined from the condition of the real propagation constant.
d) The gain model, based on the Fermi's Golden Rule [17], gives information about the optical gain spectra. A brief description of the theoretical model for calculating the optical gain and electronic band structures of the strained QW active regions may be found in our previous publication [21].

The above well-conducted self-consistent approach allows us integration of various physical phenomena taking place within a VCSEL device.

4. The parameters

4.1. Material parameters used in the electrical model. Electrical conductivities of the n- and p-type semiconductor materials are calculated from Eqs. (1) and (2) given in [22]:

$$\sigma_n = en\mu_n, \tag{1}$$

$$\sigma_p = ep\mu_p, \tag{2}$$

where e is the electron charge, n and p are the free electron and hole concentrations, μ_n and μ_p are the electron and hole mobility.

Using the existing experimental data [23–31], we obtain the following expressions for the electron mobility in Si-doped GaAs and $Al_xGa_{1-x}As$:

$$\mu_{\text{n - GaAs:Si}} = \frac{6600\dfrac{\text{cm}^2}{\text{V}\cdot\text{s}}}{1+\left(\dfrac{n}{5\cdot10^{17}\text{cm}^{-3}}\right)^{0.53}}, \tag{3}$$

$$\mu_{\text{n-AlGaAs:Si}} = \mu_{\text{n - GaAs:Si}}\cdot f(x), \tag{4}$$

$$f(x) = \begin{cases} \exp(-16x^2) & x \le 0.5, \\ 0.054x - 0.009 & x > 0.5. \end{cases} \tag{5}$$

The free electron concentrations in Si-doped GaAs and $Al_xGa_{1-x}As$ for the donor concentration N_d are approximated using the data of [23–26]:

$$n_{\text{GaAs:Si}} = N_{\text{d}}, \tag{6}$$

$$n_{\text{AlGaAs:Si}} = n_{\text{GaAs:Si}}\cdot g(x), \tag{7}$$

$$g(x) = \begin{cases} 1 - 7.8x^2 & x \le 0.35, \\ 1.14x - 0.36 & x > 0.35. \end{cases} \tag{8}$$

Using the data of [25, 32–39], we calculate electron mobility in Si- and Zn-doped InP from the following relations:

$$\mu_{\text{n - InP:Si}} = \frac{3900\dfrac{\text{cm}^2}{\text{V}\cdot\text{s}}}{1+\left(\dfrac{n}{10^{18}\text{cm}^{-3}}\right)^{0.51}}, \tag{9}$$

$$\mu_{\text{p - InP:Zn}} = \frac{120\dfrac{\text{cm}^2}{\text{V}\cdot\text{s}}}{1+\left(\dfrac{p}{2\cdot 10^{18}\text{cm}^{-3}}\right)}. \tag{10}$$

On the basis of the experimental data of [25, 40], we assume zero activation energy in Si-doped InP:

$$n_{\text{InP:Si}} = N_{\text{d}}. \tag{11}$$

The relation between the free hole concentration in Zn-doped InP and the acceptor concentration N_a is taken from [39]:

$$p_{\text{InP:Zn}} = 0.75N_{\text{a}}. \tag{12}$$

The electron mobility in Si- and Zn-doped $Ga_{0.47}In_{0.53}As$ are approximated using the data of [41–46]:

$$\mu_{\text{n - GaInAs:Si}} = \frac{16700\dfrac{\text{cm}^2}{\text{V}\cdot\text{s}}}{1+\left(\dfrac{n}{6\cdot 10^{16}\text{cm}^{-3}}\right)^{0.42}}, \tag{13}$$

$$\mu_{\text{p - GaInAs:Zn}} = \frac{250\dfrac{\text{cm}^2}{\text{V}\cdot\text{s}}}{1+\left(\dfrac{p}{6\cdot 10^{17}\text{cm}^{-3}}\right)^{0.34}}. \tag{14}$$

Using the data of [40, 44, 47], we write the following relations between free carrier and dopant concentrations in Si- and Zn-doped $Ga_{0.47}In_{0.53}As$:

$$n_{\text{GaInAs:Si}} = 0.55N_{\text{d}}, \tag{15}$$

$$p_{\text{GaInAs:Zn}} = 0.90N_{\text{a}}. \tag{16}$$

The rest of the electrical conductivities used in our model are equal to $3\cdot10^{-3}\Omega^{-1}\text{m}^{-1}$ for the α-Si [48], to $1\cdot10^{-8}\ \Omega^{-1}\text{m}^{-1}$ for the SiO_2 [49], to $1.392\cdot10^{7}\ \Omega^{-1}\text{m}^{-1}$ for the indium solder [50], to $5.794\cdot10^{7}\ \Omega^{-1}\text{m}^{-1}$ for the copper heat sink [51], and to 5 $\Omega^{-1}\text{m}^{-1}$ for the TJ [52]. We also assumed that contact resistances are equal to $2.5\cdot10^{-6}\ \Omega\text{cm}^2$ [53].

The monomolecular A, the bimolecular B, the Auger C, and the ambipolar D recombination coefficients used in the simulation are taken from [54] and are equal to: $1\cdot10^{-8}\ \text{s}^{-1}$, $4\cdot10^{-10}\ \text{cm}^3\text{s}^{-1}$, $2.43\cdot10^{-28}\ \text{cm}^6\text{s}^{-1}$, and 10 cm^2s^{-1}, respectively.

In our calculations, for RT threshold VCSEL operation, we assumed that electrical parameters does not depend on the temperature. Their RT values are listed in Table 1.

4.2. Material parameters used in the thermal model. RT thermal conductivities for InP, AlGaAs, GaInAs, GaInAsP and AlGaInAs (Table 1) are calculated from thermal resistivities for binaries given in [55–59] using interpolation formulas found in [60] and bowing parameters taken from [61-66]. Their temperature dependences and analogous expressions for α-Si, SiO_2 and copper may be found in [67]. Because of extremely thin QW layers, the whole active region is assumed to exhibit the thermal conductivity of the barriers. For the indium solder we used the constant value equal to 84 $\text{Wm}^{-1}\text{K}^{-1}$ [68].

Table 1
RT electrical σ and thermal k conductivities used in the simulation of the 2.33-μm QW TJ-VCSELs

material	σ ($\Omega^{-1}\text{m}^{-1}$)	k ($\text{Wm}^{-1}\text{K}^{-1}$)
$\alpha-$Si	$3\cdot10^{-3}$	0.98
SiO_2	$1\cdot10^{-8}$	1.44
n^+-$Ga_{0.47}In_{0.53}As$	122933	4.41
n-InP (laser A)	18354	68.03
p-InP (laser A)	607	68.03
n-$Ga_{0.47}In_{0.53}As$ (laser B)	25413	4.41
p-$Ga_{0.47}In_{0.53}As$ (laser B)	945	4.41
tunnel junction	5	4.13
n-GaAs	26436	44.05
n-$Al_{0.90}Ga_{0.10}As$	2081	25.53
n-GaAs substrate	68555	44.05

4.3. Material parameters used in the gain model. RT values and temperature dependencies of the band parameters for binaries and the bowing coefficients used in the gain calculations are taken from [69–72]. Interpolation schemes for the ternary and quaternary alloys are given in [73] and [74]. The energy gap and the electron effective mass in GaInNAs have been calculated using formulas taken from [75] and [21], respectively. RT values of the most important parameters used in the gain calculations are listed in Table 2.

Table 2
RT parameters used to determine gain spectra in the simulation of the 2.33-μm QW TJ-VCSELs

parameter	unit	value (laser A)	value (laser B)
QW energy gap	eV	0.420	0.420
QW depth in conduction band	eV	0.346	0.413
QW depth in valance band	eV	0.188	0.121
waveguide depth in conduction band	eV	0.200	-0.137
waveguide depth in valence band	eV	0.199	-0.080
spin-orbit splitting	eV	0.360	0.360
Lorentz broadening	ps	0.1	0.1
QW refractive index	-	3.8	3.8
QW electron effective mass	m_0	0.074	0.074
QW heavy hole effective mass	m_0	0.284	0.284
QW light hole effective mass	m_0	0.038	0.038
barrier electron effective mass	m_0	0.052	0.050
barrier heavy hole effective mass	m_0	0.323	0.318
barrier light hole effective mass	m_0	0.076	0.069

4.4. Material parameters used in the optical model. The refractive indices for 2.33-μm wavelength used in our model are equal to 3.328 for GaAs [76], to 2.911 for $Al_{0.90}Ga_{0.10}As$ [77], to 3.120 for InP [78], to 3.2 for $Ga_{0.47}In_{0.53}As$ [79], to 3.6 for α-Si [80], to 1.433 for SiO_2 [81], to 3.405 for AlGaInAs TJ [82], to 3.440 for AlGaInAs barrier [82], to 3.36 for GaInAsP barrier [83], and to 3.8 for GaInNAs QW [84].

The absorption coefficient in n-GaAs is approximated using the data of [85]:

$$\alpha_{\text{n - GaAs}} = 5.1\ \text{cm}^{-1}\left(\frac{n}{10^{18}\ \text{cm}^{-3}}\right)^{1.3}. \tag{17}$$

We assume that the absorption coefficient in n-AlGaAs can be obtained from linear interpolation of the absorption coefficients in GaAs and AlAs:

$$\alpha_{\text{n - AlGaAs}} = x\alpha_{\text{n - AlAs}} + (1-x)\alpha_{\text{n - GaAs}}. \quad (18)$$

Using the data of [86] we also assume that:

$$\alpha_{\text{n - AlAs}} = 0.5\alpha_{\text{n - GaAs}}. \quad (19)$$

The absorption coefficients in n- and p-InP are approximated using the data taken from [87–89].

$$\alpha_{\text{n - InP}} = 2\ \text{cm}^{-1}\left(\frac{n}{10^{18}\ \text{cm}^{-3}}\right), \quad (20)$$

$$\alpha_{\text{p - InP}} = 52\ \text{cm}^{-1}\left(\frac{p}{10^{18}\ \text{cm}^{-3}}\right)^{1.2}. \quad (21)$$

The relations between the absorptions coefficients in n- and p-$Ga_{0.47}In_{0.53}As$ and free carrier concentrations are taken from [90]:

$$\alpha_{\text{n - GaInAs}} = 4.48\ \text{cm}^{-1}\left(\frac{n}{10^{18}\ \text{cm}^{-3}}\right), \quad (22)$$

$$\alpha_{\text{p - GaInAs}} = 7.97\ \text{cm}^{-1}\left(\frac{p}{10^{17}\ \text{cm}^{-3}}\right). \quad (23)$$

Absorption coefficients for α-Si and SiO_2 can be neglected [91,92]. For the p^{++}-AlGaInAs/n^{++}-AlGaInAs TJ the absorption coefficients are assumed to be equal to 1000 cm^{-1} and 100 cm^{-1}, respectively. The latter value is also assumed for the absorption coefficients of the AlGaInAs and GaInAsP barriers.

5. The results

For an application of the considered VCSELs as a sources of the carrier wave used in the gas-sensing applications, it is of primary importance to obtain the stable single-fundamental-mode LP_{01} emission. Although in the TJ-VCSELs, contrary to oxide-confined devices, it may be achieved even for large diameters, we restrict our discussion to TJs with small diameters for which, as it will be shown later, threshold currents are relatively low. Wavelengths of the LP_{01} modes as a function of the TJ diameters and number of QWs are plotted in Figs. 3 and 4. As one can see, although increases in the TJ size and in the number of QWs cause an increase in the emitted wavelength, for all calculated cases, both the simulated lasers show LP_{01} operation with emission wavelength close to the 2.33 μm emission and can cover strong absorption line of CO.

An increase in the emitted wavelength due to modifications of the TJ diameter or number of QWs is followed by reduction of the threshold gain (Figs. 5 and 6). The calculated threshold-gain values for both lasers are comparable, however for the laser with GaInAs spacers it was impossible to achieve threshold operation for TJ with diameter smaller than 4 μm and for active region with single QW. The main reason for that result are higher temperatures (Figs. 7 and 8) obtained in the above laser caused by the low thermal conductivity (4.4 $Wm^{-1}K^{-1}$) of GaInAs spacers. In comparison, the thermal conductivity of InP is equal to 68 $Wm^{-1}K^{-1}$.

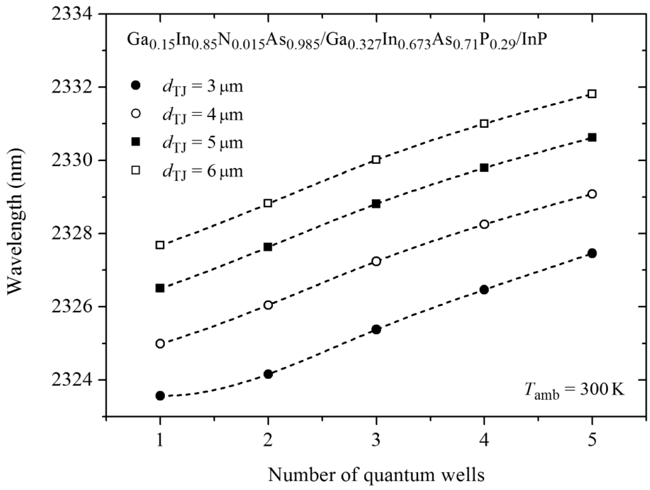

Fig. 3. RT dependence of the lasing wavelength as a function of the number of QWs determined for various TJ diameters of GaInNAs/GaInAsP/InP QW 2.33-μm VCSEL

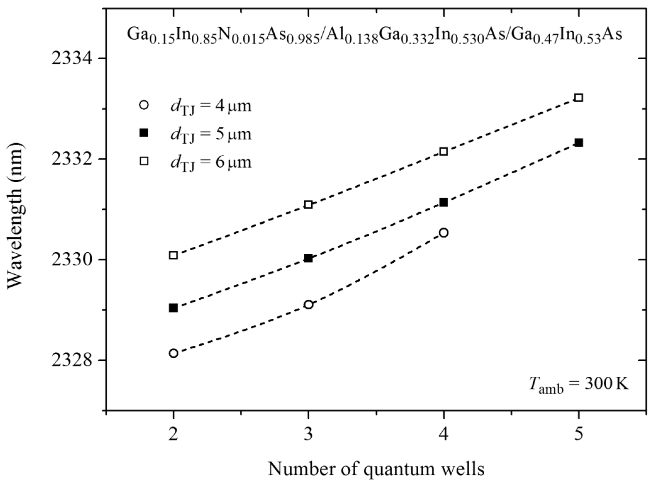

Fig. 4. RT dependence of the lasing wavelength as a function of the number of QWs determined for various TJ diameters of GaInNAs/AlGaInAs/GaInAs QW 2.33-μm VCSEL

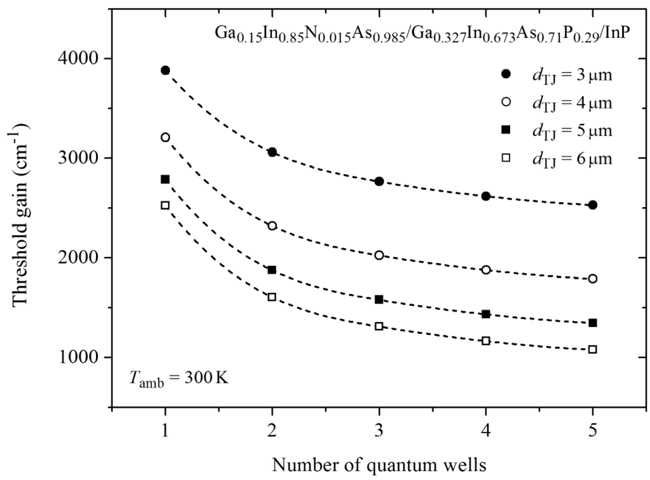

Fig. 5. RT dependence of the threshold gain as a function of the number of QWs determined for various TJ diameters of GaInNAs/GaInAsP/InP QW 2.33-μm VCSEL

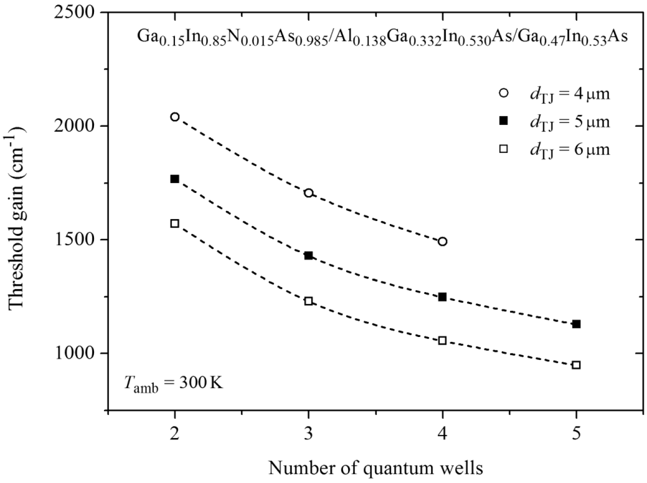

Fig. 6. RT dependence of the threshold gain as a function of the number of QWs determined for various TJ diameters of GaInNAs/AlGaInAs/GaInAs QW 2.33-μm VCSEL

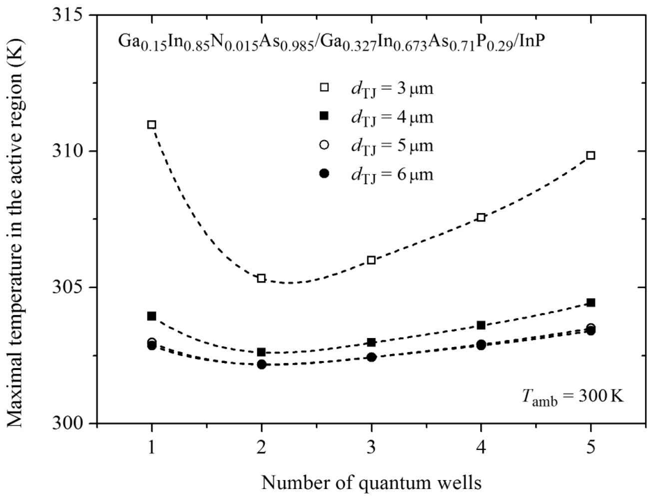

Fig. 7. Maximal temperature in the active region as a function of the number of QWs determined for various TJ diameters of GaInNAs/GaInAsP/InP QW 2.33-μm VCSEL

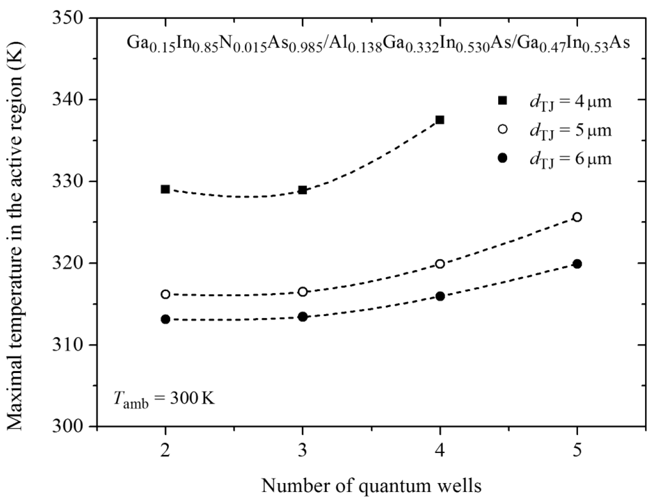

Fig. 8. Maximal temperature in the active region as a function of the number of QWs determined for various TJ diameters of GaInNAs/AlGaInAs/GaInAs QW 2.33-μm VCSEL

To determine the optimal structures of the possible GaInNAs QW TJ-VCSELs, the threshold currents for various TJ diameters and numbers of QWs were calculated. As can be seen from Fig. 9, for the laser with InP spacers, the lowest thresholds were obtained for the TJ diameter equal to 4 μm. In this case, for the active region with two QWs, the calculated threshold current was as low as 0.85 mA. Noticeably higher threshold currents were obtained for the laser with GaInAs spacers (Fig. 10). The optimal TJ diameter and number of QWs for this VCSEL were equal to 5 μm and 2, respectively, and the lowest threshold current was close to 1.7 mA.

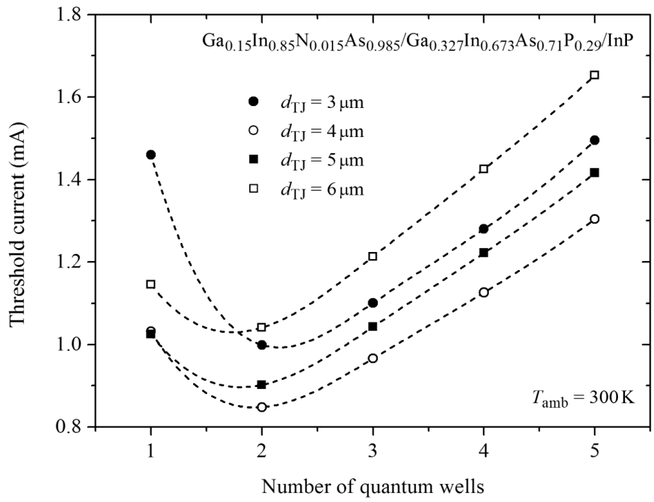

Fig. 9. RT dependence of the CW threshold current as a function of the number of QWs determined for various TJ diameters of GaInNAs/GaInAsP/InP QW 2.33-μm VCSEL

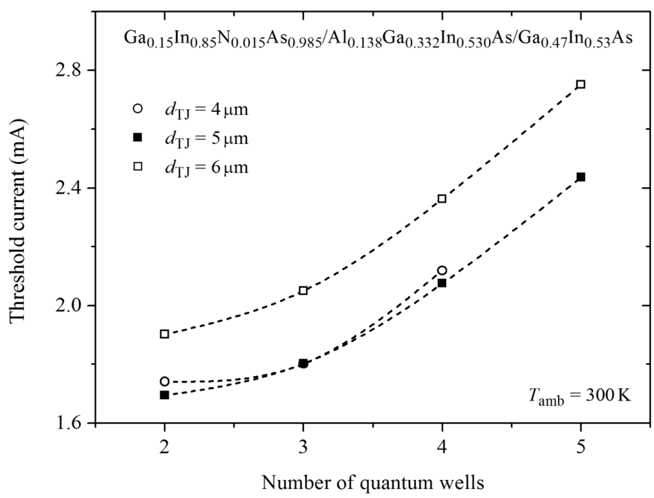

Fig. 10. RT dependence of the CW threshold current as a function of the number of QWs determined for various TJ diameters of GaInNAs/AlGaInAs/GaInAs QW 2.33-μm VCSEL

6. Conclusions

We have used the comprehensive fully self-consistent optical-electrical-thermal-recombination model to determine the optimal structure of the possible GaInNAs QW TJ VCSELs with single-fundamental-mode operation at 2.33 μm wavelength suited for CO detectors. We found that for GaInNAs/GaInAsP

QW TJ-VCSELs with InP spacers it is possible to obtain a RT CW lasing with the threshold current lower than 1 mA, which is similar to that of GaSb-based TJ-VCSELs. Higher threshold currents were obtained for laser with GaInNAs/AlGaInAs active region surrounded by the GaInAs spacers, but this structure can be grown in reactors without P source which are used for fabrication of GaAs-based devices. Both the simulated VCSELs are very promising RT CW laser sources of the 2.33-nm carrier wave for the CO-sensing applications and can represent an alternative choice to GaSb-based lasers.

Acknowledgements. This work has been supported by the COST Action MP0805 and by the Polish Ministry of Science and Higher Education, grant No N N515 533338.

REFERENCES

[1] S. Ochelski, P. Bogusz, and A. Kiczko, "Heat effects measurements in process of dynamic crash of polymer composites", *Bull. Pol. Ac.: Tech.* 60 (1), 25–30 (2012).

[2] J. Wojtas, J. Mikolajczyk, M. Nowakowski, B. Rutecka, R. Medrzycki, and Z. Bielecki, "Applying CEAS method to UV, VIS, and IR spectroscopy sensors", *Bull. Pol. Ac.: Tech.* 59 (4), 415–418 (2011).

[3] Z. Yin and X. Tang, "A review of energy bandgap engineering in III–V semiconductor alloys for mid-infrared laser applications", *Solid-State Electron.* 51 (1), 6–15 (2007).

[4] W. Both, A.E. Bochkarev, A.E. Drakin, and B.N. Sverdlov, "Thermal resistivity of quaternary solid solutions InGaAsSb and GaAlAsSb lattice-matched to GaSb", *Cryst. Res. Technol.* 24 (9), K161–K166 (1989).

[5] M. Guden and J. Piprek, "Material parameters of quaternary III–V semiconductors for multilayer mirrors at 1.55 μm wavelength", *Modell. Simul. Mater. Sci. Eng.* 4 (4), 349–357 (1996).

[6] G. Almuneau, E. Hall, T. Mukaihara, S. Nakagawa, C. Luo, D.R. Clarke, and L.A. Coldren, "Improved electrical and thermal properties of InP-AlGaAsSb Bragg mirrors for long-wavelength vertical-cavity lasers", *IEEE Photon. Techn. Lett.* 12 (10), 1322–1324 (2000).

[7] T. Borca-Tasciuc, D.W. Song, J.R. Meyer, I. Vurgaftman, M.-J. Yang, B.Z. Nosho, L.J. Whitman, H. Lee, U. Martinelli, G.W. Turner, M.J. Manfra, and G. Chen, "Thermal conductivity of $AlAs_{0.07}Sb_{0.93}$ and $Al_{0.9}Ga_{0.1}As_{0.07}Sb_{0.93}$ alloys and $(AlAs)_1/(AlSb)_{11}$ digital-alloy superlattices", *J. Appl. Phys.* 92 (9), 4994–4998 (2002).

[8] T. Newell, X. Wu, A.L. Gray, S. Dorato, H. Lee, and L.F. Lester, "The effect of increased valence band offset on the operation of 2 μm GaInAsSb-AlGaAsSb lasers", *IEEE Photon. Technol. Lett.* 11 (1), 30–32 (1999).

[9] L. Shterengas, G.L. Belenky, J.G. Kim, and R.U. Martinelli, "Design of high-power room-temperature continuous-wave GaSb-based type-I quantum-well lasers with $\lambda > 2.5$ μm", *Semicond. Sci. Tech.* 19 (5), 655–658 (2004).

[10] S. Abdollahi Pour, B.-M. Nguyen, S. Bogdanov, E.K. Huang, and M. Razeghi, "Demonstration of high performance long wavelength infrared type-II InAs/GaSb superlattice photodiode grown on GaAs substrate", *Appl. Phys. Lett.* 95 (17), 173505 (2009).

[11] H.-P.D. Yang, C. Lu, R. Hsiao, C. Chiou, C. Lee, C. Huang, H. Yu, C. Wang, K. Lin, N.A. Maleev, A.R. Kovsh, C. Sung, C. Lai, J. Wang, J. Chen, T. Lee, and J.Y. Chi, "Characteristics of MOCVD- and MBE-grown InGa(N)As VCSELs", *Semicond. Sci. Technol.* 20 (8), 834–839 (2005).

[12] L.S. Rothman, I.E. Gordon, A. Barbe, D.C. Benner, P.F. Bernath, M. Birk, V. Boudon, L.R. Brown, A. Campargue, J.-P. Champion, K. Chance, L.H. Coudert, V. Dana, V.M. Devi, S. Fally, J.-M. Flaud, R.R. Gamache, A. Goldman, D. Jacquemart, I. Kleiner, N. Lacome, W.J. Lafferty, J.-Y. Mandin, S.T. Massie, S.N. Mikhailenko, C.E. Miller, N. Moazzen-Ahmadi, O.V. Naumenko, A.V. Nikitin, J. Orphal, V.I. Perevalov, A. Perrin, A. Predoi-Cross, C.P. Rinsland, M. Rotger, M. Šimečková, M.A.H. Smith, K. Sung, S.A. Tashkun, J. Tennyson, R.A. Toth, A.C. Vandaele, and J. Vander Auwera, "The HITRAN 2008 molecular spectroscopic database", *J. Quant. Spectrosc. Radiat. Transfer* 110 (9–10), 533–572 (2009).

[13] A. Bachmann, K. Kashani-Shirazi, S. Arafin, and M.-C. Amann, "GaSb-based VCSEL with buried tunnel junction for emission around 2.3 μm", *IEEE J. Sel. Topics Quantum Electron.* 15 (3), 933–940 (2009).

[14] M.-C. Amann, S. Arafin, and K. Vizbaras, "Single mode and tunable GaSb-based VCSELs for wavelengths above 2 μm", *Proc. SPIE* 7952, 7952–12 (2011).

[15] S. Ara?n, A. Bachmann, K. Vizbaras, A. Hangauer, J. Gustavsson, J. Bengtsson, A. Larsson, and M.-C. Amann, "Comprehensive analysis of electrically-pumped GaSb-based VCSELs", *Opt. Express* 19 (18), 17267–17282 (2011).

[16] R.P. Sarzała, "Modelling of the threshold operation of 1.3-μm GaAs-based oxide-confined (InGa)As/GaAs quantum-dot vertical-cavity surface-emitting lasers", *IEEE J. Quantum Electron.* 40 (6), 629–639 (2004).

[17] R.P. Sarzała and W. Nakwaski, "Optimisation of the 1.3-μm GaAs-based oxide-confined (GaIn)(NAs) vertical-cavity surface-emitting lasers for their low-threshold room-temperature operation", *J. Phys.: Condens. Mat.* 16 (31), S3121–S3140 (2004).

[18] R.P. Sarzała, M. Wasiak, T. Czyszanowski, and W. Nakwaski, "Performance characteristics of the 1.3-μm oxide-confined edge-emitting quantum-dot (InGa)As/GaAs diode lasers", *Bull. Pol. Ac.: Tech.* 52 (3), 257–263 (2004).

[19] A. Tomczyk, R.P. Sarzała, T. Czyszanowski, M. Wasiak, and W. Nakwaski, "Fully self-consistent three-dimensional model of edge-emitting nitride diode lasers", *Opto-Electron. Rev.* 11 (1), 65–75 (2003).

[20] H. Wenzel and H.J. Wünsche, "The effective frequency method in the analysis of vertical-cavity surface-emitting lasers", *IEEE J. Quantum Electron.* 33 (7), 1156–1162 (1997).

[21] R.P. Sarzała, Ł. Piskorski, P. Szczerbiak, R. Kudrawiec, and W. Nakwaski, "An attempt to design long-wavelength (> 2 μm) InP-based GaInNAs diode lasers", *Appl. Phys.* A 108 (3), 521–528 (2012).

[22] H. Czichos, T. Saito, and L.M. Smith, *Springer Handbook of Materials Measurement Methods*, Springer, Berlin, 2006.

[23] T. Ishikawa, J. Saito, S. Sasa, and S. Hiyamizu, "Electrical properties of Si-doped $Al_xGa_{1-x}As$ layers grown by MBE", *Jpn. J. Appl. Phys.* 21 (11), L675–L676 (1982).

[24] M.L. Lovejoy, M.R. Melloch, and M.S. Lundstrom, "Temperature dependence of minority and majority carrier mobilities in degenerately doped GaAs", *Appl. Phys. Lett.* 67 (8), 1101–1103 (1995).

[25] S. Izumi, N. Hayafuji, K. Ito, K. Sato, and M. Otsubo, "Chemical beam epitaxial growth of Si doped GaAs and InP by using silicon tetraiodide", *Appl. Phys. Lett.* 68 (22), 3102–3104 (1996).

[26] N. Chand, T. Henderson, J. Klem, W.T. Masselink, R. Fischer, Y.-C. Chang, and H. Morkoc, "Comprehensive analysis of Si-doped $Al_xGa_{1-x}As$ ($x = 0$ to 1): theory and experiments", *Phys. Rev.* B 30 (8), 4481–4492 (1984).

[27] T.F. Kuech, B.S. Meyerson, and E. Veuhoff, "Disilane: a new silicon doping source in metalorganic chemical vapour deposition of GaAs", *Appl. Phys. Lett.* 44 (10), 986–988 (1984).

[28] J. Saito and K. Kondo, "High-temperature growth of Si-doped AlGaAs by molecular-beam epitaxy", *J. Vac. Sci. Technol.* B 8 (6), 1264–1269 (1990).

[29] P.R. Hageman, M.H.J.M. de Croon, J.N.H. Reek, and L.J. Giling, "Pressure and temperature dependence os silicon doping of GaAs using Si2H6 in metalorganic chemical vapour deposition", *J. Cryst. Growth* 116 (1–2), 169–177 (1992).

[30] K. Tateno and C. Amano, "Carbon doping and etching in $Ga_xIn_{1-x}As_yP_{1-y}$ on GaAs substrates using CBr_4 by metalorganic chemical vapor deposition", *J. Electron. Mater.* 28 (1) 63–68 (1999).

[31] V. Bondarenko, "Positron annihilation study of equilibrium point defects in GaAs", *PhD Thesis*, Martin Luther University of Halle- Wittenberg, Wittenberg, 2003.

[32] C. Blaauw, F.R. Shepherd, C.J. Miner, and A.J. Springrhorpe, "Silicon incorporation in InP during LP-MOCVD using disilane", *J. Electron. Mater.* 19 (1), 1–6 (1990).

[33] J.N. Baillargeon, A.Y. Cho, and R.J. Fischer, "Growth of silicon and beryllium doped InP by MBE using solid phosphorus", *Proc. 6th Int. Conf. on Indium Phosphide and Related Materials* CA, 148–150 (1994).

[34] J.M. Milikow, "Growth and characterization of III-V compound semiconductors", *MSc Thesis*, Massachusetts Institute of Technology, Massachusetts, 1997.

[35] Ch. Giesen, X.G. Xu, R. Hövel, M. Heuken, and K. Heime, "Silicon doping of InP grown by MOVPE using tertiarybutylphosphine", *Proc. 9th Int. Conf. on Indium Phosphide and Related Materials* MA, 47–50 (1997).

[36] K. Radhakrishnan, H.Q. Zheng, P.H. Zhang, S.F. Yoon, and G.I. Ng, "Characterization of silicon-doped InP grown by solid-source molecular beam epitaxy using a valved phosphorus cracker cell", *J. Cryst. Growth* 204 (3), 275–281 (1999).

[37] F.G. Kellert and S.R. Sloan, "Zn-doping in OMVPE grown InP:Zn/InGaAs/InP $p-i-n$ double heterojunctions with InGaAs:Zn contacting layers", *J. Electron. Mater.* 21 (10), 983–987 (1992).

[38] B. Pődör, "Hole mobility in InP and GaSb", *Proc. 31st Int. Spring Seminar on Electronics Technology* 1, 201–204 (2008).

[39] C.A.C. Sequeira and D.M.F. Santos, "Hall effect measurements on p-n-p InP structures", *Braz. J. Phys.* 38 (1), 147–155 (2008).

[40] K. Beer, B. Baur, H. Heinecke, and R. Treichler, "Improvements in silicon doping of InP and GaInAs in metalorganic molecular beam epitaxy", *J. Cryst. Growth* 120 (1–4), 312–316 (1992).

[41] K.Y. Cheng and A.Y. Cho, "Silicon doping and impurity profiles in $Ga_{0.47}In_{0.53}As$ and $Al_{0.48}In_{0.52}As$ grown by molecular beam epitaxy", *J. Appl. Phys.* 53 (6), 4411–4415 (1982).

[42] R.A. Kubiak, J.J. Harris, and P. Dawson, "Electrical and optical properties of Si and Sn doped $In_xGa_{1-x}As$ (x = 0.53) grown by molecular beam epitaxy", *J. Appl. Phys.* 55 (2), 598–600 (1984).

[43] T. Fujii, T. Inata, K. Ishii, and S. Hiyamizu, "Heavily Si-doped InGaAs lattice-matched to InP grown by MBE", *Electron. Lett.* 22 (4), 191–192 (1986).

[44] N. Watanabe, T. Nittono, and K. Watanabe, "Annealing effect on the carrier concentration in heavily Si-doped n^+-InGaAs", *Appl. Phys. Lett.* 61 (16), 1945–1947 (1992).

[45] D. Suzuki, T. Kimura, T. Takiguchi, M. Takemi, S. Fuji, Y. Mihashi, and H. Higuchi, "MOCVD growth of heavily p-type doped InGaAs using bismethylcyclopentadienylberyllium", *Proc. Int. Conf. on Indium Phosphide and Related Materials* MA, 540–543 (1997).

[46] C. Chelli, D. Cui, S.M. Hubbard, A. Eisenbach, D. Pavlidis, S.K. Krawczyk, and B. Sermage, "Minority carrier lifetime in MOCVD-grown C- and Zn-doped InGaAs", *Proc. 11th Int. Conf. on Indium Phosphide and Related Materials* 1, 127–130 (1999).

[47] T. Sato, M. Mitsuhara, R. Iga, S. Kanazawa, and Y. Inoue, "Zn-doped InGaAs with high carrier concentration enhanced by Sb surfactant for low specific contact resistance", *Proc. Int. Conf. on Indium Phosphide and Related Materials* 1, 1–4 (2010).

[48] P.G. Le Comber and J. Mort, *Electronic and Structural Properties of Amorphous Semiconductors*, Academic Press, New York, 1973.

[49] J.F. Shackelford and W. Alexander, *CRC Materials Science and Engineering Handbook*, CRC Press, London, 2001.

[50] www.thinfilm.com

[51] D.R. Lide, *CRC Handbook of Chemistry and Physics*, Internet Version, Boca Raton, 2005.

[52] Ł. Piskorski, R.P. Sarzała, and W. Nakwaski, "Investigation of temperature characteristics of modern InAsP/InGaAsP multiquantum-well TJ-VCSELs for optical fibre communication", *Opto-Electron. Rev.* 19 (3), 320–326 (2011).

[53] O. Dier, C. Lauer, and M.-C. Amann, "n-InAsSb/p-GaSb tunnel junctions with extremely low resistivity", *Electron. Lett.* 42 (7), 419–420 (2006).

[54] P. Szczerbiak, "The model of the diode laser emitting in the mid-infrared region with the dilute-nitride active region on indium phosphide", *BSc Thesis*, Lodz University of Technology, Łódź, 2011, (in Polish).

[55] E.F. Steigmeier and I. Kudman, "Thermal conductivity of III-V compounds at high temperatures", *Phys. Rev.* 132 (2), 508–512 (1963).

[56] I. Kudman and E.F. Steigmeier, "Thermal conductivity and Seebeck coefficient of InP", *Phys. Rev.* 133 (6A), A1665–A1667 (1964).

[57] S. Amith, I. Kudman, and E.F. Steigmeier, "Electron and phonon scattering in GaAs at high temperatures", *J. Appl. Phys.* 138 (4A), A1270–A1276 (1965).

[58] E.F. Steigmeier and I. Kudman, "Acoustical-optical phonon scattering in Ge, Si, and III-V compounds", *Phys. Rev.* 141 (2), 767–774 (1966).

[59] M.A. Afromowitz, "Thermal conductivity of $Ga_{1-x}Al_xAs$ alloys", *J. Appl. Phys.* 44 (3), 1292–1294 (1973).

[60] W. Nakwaski, "Thermal conductivity of binary, ternary, and quaternary III-V compounds", *J. Appl. Phys.* 64 (1), 159–166 (1988).

[61] R. Bowers, J.E. Bauerle, and A.J. Cornish, "$InAs_{1-x}P_x$ as a thermoelectric material", *J. Appl. Phys.* 30 (7), 1050–1054 (1959).

[62] M.S. Abrahams, R. Braunstein, and F.D. Rosi, "Thermal, electrical and optical properties of (In,Ga)as alloys", *J. Phys. Chem. Solids* 10 (2–3), 204–210 (1959).

[63] B. Abeles, "Lattice thermal conductivity of disordered semiconductor alloys at high temperatures", *Phys. Rev.* 131 (5), 1906–1911 (1963).

[64] R.O. Carlson, G.A. Slack, and S.J. Silverman, "Thermal conductivity of GaAs and $GaAs_{1-x}P_x$ laser semiconductors", *J. Appl. Phys.* 36 (2), 505–507 (1965).
[65] W. Both and F.P. Herrmann, "Thermal resistivity of quaternary solid solution $Ga_xIn_{1-x}As_yP_{1-y}$ lattice-matched to InP and GaAs", *Cryst. Res. Technol.* 17 (11), K117–K122 (1982).
[66] N. Yacoubi, B. Girault, and J. Fesquet, "Determination of absorption coefficients and thermal conductivity of GaAlAs/GaAs heterostructure using a photothermal method", *Appl. Optics* 25 (24), 4622–4625 (1986).
[67] Ł. Piskorski, "Modelling of physical phenomena in the selected VCSEL structures emitting at the second telecommunication window wavelength", *PhD Thesis*, Lodz University of Technology, Łódź, 2010, (in Polish).
[68] www.lakeshore.com
[69] I. Vurgaftman, J.R. Meyer, and L.R. Ram-Mohan, "Band parameters for III-V compound semiconductors and their alloys", *J. Appl. Phys.* 89 (11), 5815–5875 (2001).
[70] I. Vurgaftman and J.R. Meyer, "Band parameters for nitrogen-containing semiconductors", *J. Appl. Phys.* 94 (6), 3675–3696 (2003).
[71] S. Wang, "Studies on thermodynamic properties of III-V compounds by first-principles response-function calculation", *Phys. Stat. Sol.* B 246 (7), 1618–1627 (2009).
[72] S. Adachi S, *Properties of Semiconductor Alloys: Group-IV, III-V and II-VI Semiconductors*, John Wiley & Sons, Chichester, 2009.
[73] T.H. Glisson, J.R. Hauser, M.A. Littlejohn, and C.K. Williams, "Energy bandgap and lattice constant contours of iii-v quaternary alloys", *J. Electron. Mater.* 7 (1), 1–16 (1978).
[74] C.K. Williams, T.H. Glisson, J.R. Hauser, and M.A. Littlejohn, "Energy bandgap and lattice constant contours of iii-v quaternary alloys of the form $A_xB_yC_zD$ or $AB_xC_yD_z$", *J. Electron. Mater.* 7 (5), 639–646 (1978).
[75] R. Kudrawiec, Alloying of GaN_xAs_{1-x} with InN_xAs_{1-x}: a simple formula for the bandgap parametrization of $Ga_{1-y}In_yN_xAs_{1-x}$ alloys", *J. Appl. Phys.* 101 (2), 023522 (2007).
[76] www.refractiveindex.info
[77] S. Gehrsitz, F.K. Reinhart, C. Gourgon, N. Herres, A. Vonlanthen, and H.Sigg, "The refractive index of $Al_xGa_{1-x}As$ below the band gap: accurate determination and empirical modelling", *J. Appl. Phys.* 87 (11), 7825–7837 (2000).
[78] S. Adachi, "Model dielectric constants of GaP, GaAs, GaSb, InP, InAs, and InSb", *Phys. Rev.* B 35 (14), 7454–7463 (1987).
[79] S. Adachi, *Physical Properties of III-V Semiconductor Compounds*, John Wiley & Sons, Chichester, 1992.
[80] E. Kessels, *Remote Plasma Deposition of Hydrogenated Amorphous Silicon: Plasma Processes, Film Growth and Material Properties*, Technische Universiteit Eindhoven, Eindhoven, 2000.
[81] www.filmetrics.com
[82] C. Grasse, G. Boehm, M. Mueller, T. Gruendl, R. Meyer, and M.-C. Amann, "Empirical modeling of the refractive index for (AlGaIn)As lattice matched to InP", *Semicond. Sci. Technol.* 25 (4), 045018 (2010).
[83] B. Jensen and A. Torabi, "Refractive index of quaternary $In_{1-x}Ga_xAs_yP_{1-y}$ lattice matched to InP", *J. Appl. Phys.* 54 (6), 3623–3625 (1983).
[84] R.P. Sarzała, Ł. Piskorski, P. Szczerbiak, W. Nakwaski, and R. Kudrawiec, "Long-wavelength InP-based GaInNAs lasers", *Proc. Eur. Materials Research Society (E-MRS) Spring Meeting* T, T-12 (2012).
[85] W.G. Spitzer and J.M. Whelan, "Infrared absorption and electron effective mass in n-type gallium arsenide", *Phys. Rev.* 114 (1), 59–63 (1959).
[86] D.I. Babic, J. Piprek, K. Streubel, R.P. Mirin, N.M. Margalit, D.E. Mars, J.E. Bowers, and E.L. Hu, "Design and analysis of double-fused 1.55-μm vertical-cavity lasers", *IEEE J. Quantum Electron.* 33 (8), 1369–1383 (1997).
[87] O.K. Kim and W.A. Bonner, "Infrared reflectance and absorption of N-type InP", *J. Electron. Mater.* 12 (5), 827–836 (1983).
[88] C.H. Henry, R.A. Logan, F.R. Merritt, and J.P. Luongo, "The effect of intervalence band absorption on the thermal behavior of InGaAsP lasers", *J. Quantum Electron.* 19 (6), 947–952 (1983).
[89] H.C. Casey and P.L. Carter, "Variation of intervalence band absorption with hole concentration in p-type InP", *Appl. Phys. Lett.* 44 (1), 82–83, 1984.
[90] D.M. Wilt, N.S. Fatemi, P.P. Jenkins, V.G. Weizer, R.W. Hoffman, Jr., R.K. Jain, Ch.S. Murray, and D.R. Riley, "Electrical and optical performance characteristics of 0.74-eV p/n InGaAs monolithic interconnected modules", *NASA Technical Memorandum* 113110, 1–10 (1997).
[91] M. Ortsiefer, C. Neumeyr, J. Rosskopf, S. Arafin, G. Böhm, A. Hangauer, J. Chen, R. Strzoda, and M.-C. Amann, "GaSb and InP-based VCSELs at 2.3 μm emission wavelength for tuneable diode laser spectroscopy of carbon monoxide", *Proc. SPIE* 7945, 7945–09 (2011).
[92] R. Kitamura, L. Pilon, and M. Jonasz, "Optical constants of silica glass from extreme ultraviolet to far infrared at near room temperature", *Appl. Optics* 46 (33), 8118–8133 (2007).